

Numerical Simulations of Two-Fluid Magnetoacoustic Waves in the Solar Atmosphere

J. Kraškiewicz¹, K. Murawski¹, and Z.E. Musielak²

¹ Institute of Physics, University of Maria Curie-Skłodowska, Pl.
Marii Curie-Skłodowskiej 5, 20-031 Lublin, Poland

² Department of Physics, University of Texas at Arlington,
Arlington, TX 76019, USA

November 30, 2022

Abstract

We study vertical variations of wave-periods of magnetoacoustic two-fluid waves in the partially ionized lower solar atmosphere, consisting of ion (proton) + electron and neutral (atomic hydrogen) fluids, which are coupled by ion-neutral collisions. The study allows finding the wave period cutoffs and their variations in the solar atmosphere, as well as establishing the role of these cutoffs in determining the wave propagation conditions. The atmosphere is permeated by a uniform vertical magnetic field. We perform numerical simulations in the framework of a one-dimensional (1D), two-fluid model in which plane waves are excited by a harmonic driver in the vertical ion and neutral velocities, operating at the bottom of the solar photosphere. We observe excitation of waves with cutoff wave-periods in addition to waves set directly by the driver. We also see that some waves excited by that driver can reach the solar corona. Despite of its limitations such as the lack of non-adiabatic and non-ideal terms and a simple 1D structure, the developed two-fluid model of the solar atmosphere sheds a new light on the role of cutoffs in setting up the wave propagation conditions in the solar atmosphere and finding periods of waves that may carry their energy from the solar surface to the corona.

Methods: numerical – Sun: chromosphere – Sun: transition region

1 INTRODUCTION

The structure of the solar atmosphere varies from partially ionized in its lower layers to fully ionized in the solar corona. In the solar photosphere there is one ion per about $10^3 - 10^4$ neutrals but in the chromosphere and in the transition region the number of neutrals rapidly falls off with height as the temperature

increases (e.g., Priest 2014; Ballester et al. 2018). The role of wave heating in this temperature increase has been investigated in many papers (e.g., Narain & Ulmschneider 1996; Roberts & Ulmschneider 1997; Roberts 1991, 2006) in which a fully ionized solar atmosphere is typically considered. Recently, the effects of partially ionized solar atmosphere on the wave propagation are taken into account in two-fluid numerical studies performed by Maneva et al. (2017), Wójcik et al. (2019), Popescu Braileanu et al. (2019), Kuźma et al. (2019) and Murawski et al. (2020). The obtained results demonstrate that ion and neutral waves behave differently and that ion-neutral collisions may become an effective damping mechanism for the waves.

The wave propagation in the solar atmosphere is strongly affected by the presence of cutoff periods, which are different for different waves and strongly depend on the structure of media in which the waves propagate. The concept of cutoff periods was originally introduced by Lamb (1909, 1910, 1945) for acoustic waves propagating in stratified but isothermal atmospheres. Then, the work was extended to more realistic (nonisothermal) atmospheres with magnetic fields in which the cutoffs for different waves were obtained analytically (e.g., Defouw 1976; Gough 1977; Rae & Roberts 1982; Musielak 1990; Fleck & Schmitz 1991, 1993; Schmitz & Fleck 1992; Stark & Musielak 1993; Musielak & Moore 1995; Roberts & Ulmschneider 1997; Roberts 2004, 2006; Musielak et al. 2006, 2007; Routh et al. 2010; Murawski & Musielak 2010; Cally & Hasan 2011; Routh & Musielak 2014; Perera et al. 2015; Felipe et al. 2018; Routh et al. 2020). All these analytical studies were done for fully ionized (and often isothermal) solar atmosphere; despite these limitations some of the derived cutoffs for acoustic and magnetoacoustic waves (MAWs) will be compared to the results for two-fluid MAWs obtained in this paper.

The above analytical studies of cutoff periods were supplemented by 3D numerical simulations of different linear and nonlinear waves in the solar atmosphere with different non-magnetic and magnetic settings, and the wave generation, propagation and dissipation were investigated. Specific numerical results involve impulsively generated linear and non-linear magnetohydrodynamic (MHD) waves, 3D simulations of magnetic twistors, and 3D simulations of magnetic flux tube waves (e.g., Murawski & Zaqarashvili 2010; Chmielewski et al. 2013; Murawski et al. 2016; Martínez-Sykora et al. 2017; Maneva et al. 2017; Kraśkiewicz et al. 2019; Kuźma et al. 2019; Popescu Braileanu et al. 2019; Wójcik et al. 2018, 2019, 2020; Murawski et al. 2020). Some of this work has already included the effects of partial ionization of the solar atmosphere. Specifically, the observationally established variations of the acoustic cutoff periods with height in the solar atmosphere (Wiśniewska et al. 2016; Kayshap et al. 2018) were partially reproduced numerically by Murawski & Musielak (2016), Murawski et al. (2016); however, recently Kuźma et al. (2022) obtained a very good agreement with the observations.

The main purpose of this paper is to extend the MHD models (e.g., Fleck & Schmitz 1991, Kalkofen et al. 1994, Kraśkiewicz et al. 2019) according to which for the piston-wave excitation in the isothermal atmosphere, the asymptotic solution shows in the linear limit a superposition of waves with the piston wave-

period and waves with the cutoff wave-period. For the waves excited above the cutoff period, the atmosphere oscillates with the acoustic cutoff period at greater heights; however, as time elapses the piston driving period takes over. The extension is done to account for a non-isothermal solar atmosphere, the conditions for propagation of long wave-period two-fluid MAWs are determined by taking into account the effects of dynamics of neutrals, and by considering wave-periods of neutral waves.

The paper is organized as follows. In Sec. 2 we describe the numerical model of the atmosphere. In Sec. 3 we present our numerical results. We finalize our draft by conclusions in Sec. 4.

2 NUMERICAL MODEL OF THE SOLAR ATMOSPHERE

We consider a 1D magnetically structured and gravitationally stratified solar atmosphere which dynamics is described by set of two-fluid equations for ions + electrons treated as one fluid and neutrals regarded as second fluid. Specifically, these fluids are governed by the following equations (e.g., Maneva et al. 2017; Popescu Braileanu et al. 2019):

$$\frac{\partial \varrho_n}{\partial t} + \nabla \cdot (\varrho_n \mathbf{V}_n) = 0, \quad (1)$$

$$\frac{\partial \varrho_i}{\partial t} + \nabla \cdot (\varrho_i \mathbf{V}_i) = 0, \quad (2)$$

$$\frac{\partial (\varrho_n \mathbf{V}_n)}{\partial t} + \nabla \cdot (\varrho_n \mathbf{V}_n \mathbf{V}_n + p_n \mathbf{I}) = \varrho_n \mathbf{g} + \mathbf{S}_m, \quad (3)$$

$$\frac{\partial (\varrho_i \mathbf{V}_i)}{\partial t} + \nabla \cdot (\varrho_i \mathbf{V}_i \mathbf{V}_i + p_i \mathbf{I}) = \frac{1}{\mu} (\nabla \times \mathbf{B}) \times \mathbf{B} + \varrho_i \mathbf{g} - \mathbf{S}_m, \quad (4)$$

$$\frac{\partial \mathbf{B}}{\partial t} = \nabla \times (\mathbf{V}_i \times \mathbf{B}), \quad \nabla \cdot \mathbf{B} = 0, \quad (5)$$

$$\frac{\partial E_n}{\partial t} + \nabla \cdot [(E_n + p_n) \mathbf{V}_n] = \varrho_n \mathbf{g} \cdot \mathbf{V}_n + S_{En}, \quad (6)$$

$$\frac{\partial E_i}{\partial t} + \nabla \cdot \left[\left(E_i + p_i + \frac{\mathbf{B}^2}{2\mu} \right) \mathbf{V}_i - \frac{\mathbf{B}}{\mu} (\mathbf{V}_i \cdot \mathbf{B}) \right] = \varrho_i \mathbf{g} \cdot \mathbf{V}_i + S_{Ei}, \quad (7)$$

$$E_n = \frac{\varrho_n \mathbf{V}_n^2}{2} + \frac{p_n}{\gamma - 1}, \quad (8)$$

$$E_i = \frac{\varrho_n \mathbf{V}_i^2}{2} + \frac{\mathbf{B}^2}{2\mu} + \frac{p_i}{\gamma - 1}. \quad (9)$$

Here the momentum collisional, \mathbf{S}_m , and energy, $S_{Ei,n}$, source terms are given as

$$\mathbf{S}_m = \alpha_c(\mathbf{V}_i - \mathbf{V}_n), \quad (10)$$

$$S_{En} = \frac{1}{2}\alpha_c(V_i - V_n)^2 + \frac{3\alpha_c k_B}{m_i + m_n}(T_i - T_n) \quad (11)$$

$$S_{Ei} = \frac{1}{2}\alpha_c(V_i - V_n)^2 + \frac{3\alpha_c k_B}{m_i + m_n}(T_n - T_i) \quad (12)$$

with subscripts i, n and e corresponding respectively to ions, neutrals and electrons. The symbols $\varrho_{i,n}$ denote mass densities, $\mathbf{V}_{i,n} = [V_{i,n,x}, V_{i,n,y}, 0]$ velocities, $p_{i,n}$ ion+electron and neutral gas pressures, \mathbf{B} is magnetic field and $T_{i,n}$ are temperatures specified by ideal gas laws,

$$p_n = \frac{k_B}{m_n}\varrho_n T_n, \quad p_i = \frac{k_B}{m_i}\varrho_i T_i. \quad (13)$$

Collision coefficient is given as (e.g. Oliver et al. 2016; Ballester et al. 2018, and references cited therein)

$$\alpha_c = \frac{4}{3} \frac{\sigma_{in}}{m_i + m_n} \sqrt{\frac{8k_B}{\pi} \left(\frac{T_i}{m_i} + \frac{T_n}{m_n} \right)} \varrho_n \varrho_i \quad (14)$$

with σ_{in} being the collisional cross-section for which we have chosen its quantum value of $1.4 \times 10^{-19} \text{ m}^2$ (Vranjes and Krstic 2013). A gravity vector is $\mathbf{g} = [0, -g, 0]$ with its magnitude $g = 274.78 \text{ m s}^{-2}$, $m_{i,n}$ are the masses of respectively ions and neutrals, k_B is the Boltzmann constant, $\gamma = 5/3$ is the specific heats ratio, and μ is magnetic permeability of the medium. The other symbols have their standard meaning.

The present 1D model suffers from severe limitations. For instance, important dissipative effects such as ionization/recombination, thermal conduction and radiative losses are neglected. This leads very likely to an overestimated energy flux of these waves that can be carried into the corona. In addition, the very significant magnetic expansion of flux tubes from the photosphere to the corona is neglected, leading to severe overestimation of the wave energy flux and the corresponding density perturbations. These effects are very important since the magnetic field strength could decrease by 2 – 3 orders of magnitude from the photosphere to the corona. We plan to make our model more realistic in future studies.

2.1 Equilibrium

We assume that the equilibrium plasma is still ($\mathbf{V}_i = \mathbf{V}_n = \mathbf{0}$) and the solar atmosphere is hydrostatic, viz.

$$\varrho_{hi,n} g = - \frac{\partial p_{hi,n}}{\partial y}. \quad (15)$$

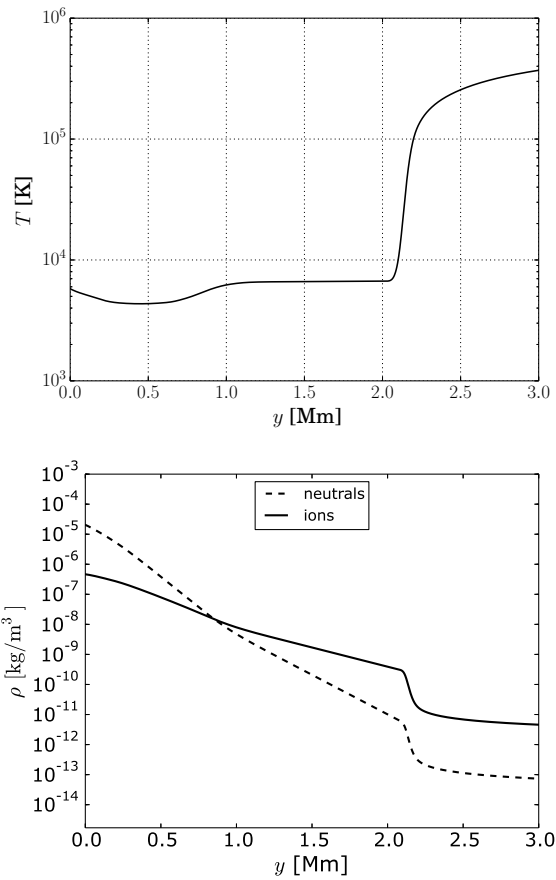


Figure 1: Vertical profiles of equilibrium temperature (top) and the hydrostatic mass densities of the ionized (bottom, solid line) and neutral fluids (bottom, dashed line) versus height, y , in the two-fluid model of the solar atmosphere.

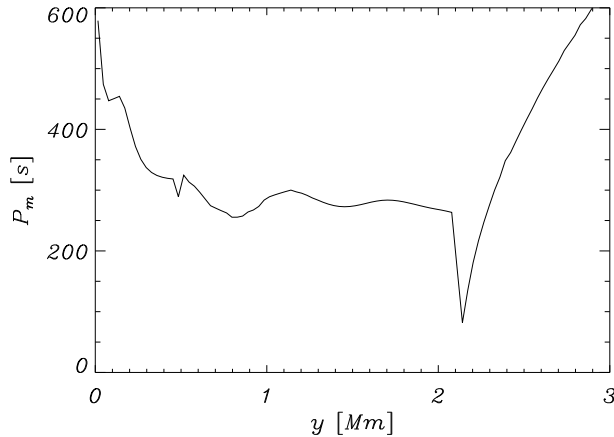


Figure 2: The cutoff wave-period, P_m , vs. height in the case of vertical magnetic field of magnitude $B_y = 11.4$ G.

This equation is satisfied by

$$p_{\text{hi},n}(y) = p_{0i,n} \exp \left[- \int_{y_r}^y \frac{dy'}{\Lambda_{i,n}(y')} \right], \quad (16)$$

$$\varrho_{\text{hi},n}(y) = \frac{p_{\text{hi},n}(y)}{g\Lambda_{i,n}(y)}, \quad (17)$$

where the subscript _h corresponds to a hydrostatic quantity, $y_r = 50$ Mm is the reference level, $p_{0i} = 10^{-2}$ Pa and $p_{0n} = 3 \cdot 10^{-4}$ Pa are, respectively, the ion and neutral gas pressure at this level and

$$\Lambda_{i,n}(y) = \frac{k_B T(y)}{m_{i,n} g} \quad (18)$$

is the ion (neutral) pressure scale-height that depends on the plasma temperature $T(y)$, which is taken from the semi-empirical model of Avrett & Loeser (2008). See Fig. 1 (top). The ion and neutral mass density profiles at the equilibrium are shown in Fig. 1 (bottom, solid line). Note that at $y = 0$ Mm, which correspond to the bottom of the photosphere, $\varrho_n \approx 30\varrho_i$. For $y > 0.7$ Mm $\varrho_i > \varrho_n$ and at $y = 3$ Mm $\varrho_i = 80\varrho_n$. The above hydrostatic equilibrium is overlaid by a current-free ($\nabla \times \mathbf{B}/\mu = \mathbf{0}$) magnetic field. We consider the case of vertical magnetic field, $\mathbf{B} = [0, B_y, 0]$ with $B_y = 11.4$ G. This value of magnetic field is typical for the solar corona and representative for the chromosphere.

2.2 Cutoff periods

For the physical settings considered in this paper, the relevant cutoff periods were derived by Roberts (2004) for acoustic waves, and by Roberts (2006) for

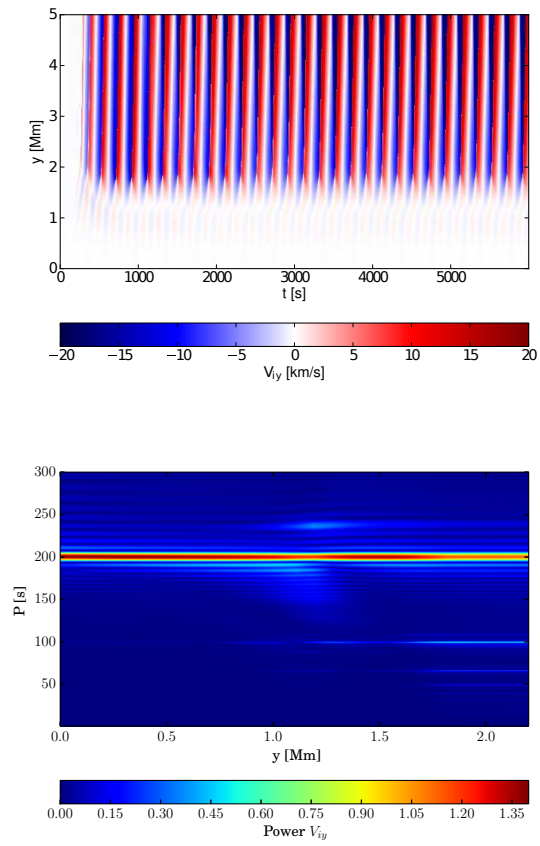


Figure 3: Time-distance plot for the ion vertical velocity, V_{iz} , (top) and its Fourier period, P , vs. height, y , (bottom) in the case of $P_d = 200$ s.

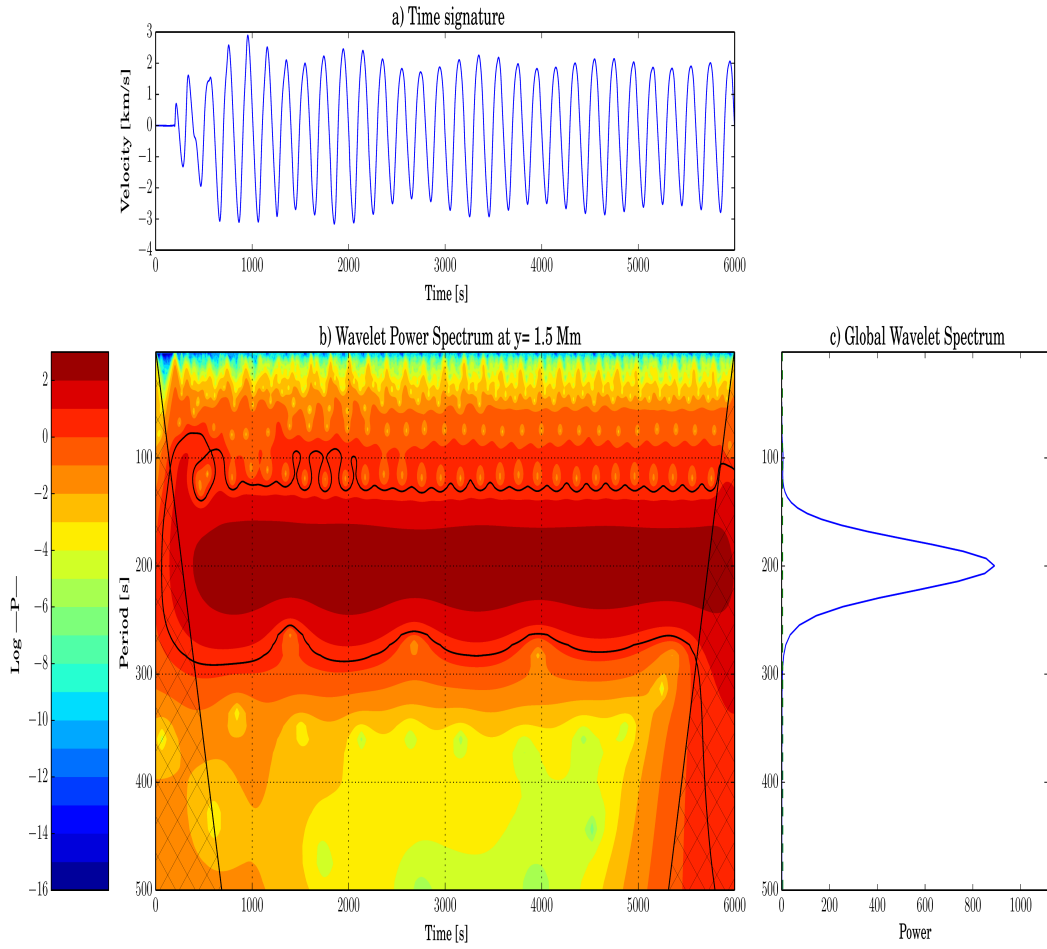


Figure 4: Time-signature for $V_{iy}(y = 1.5 \text{ Mm})$ (top), its wavelet spectrum (left-bottom), and global wavelet spectrum (right-bottom) in the case of $P_d = 200 \text{ s}$.

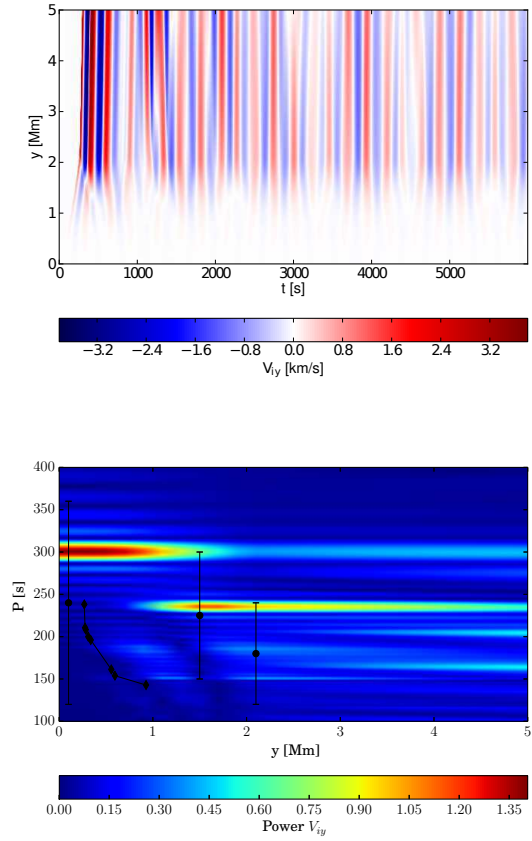


Figure 5: Time-distance plot for the ion vertical velocity, V_{iz} , (top) and its Fourier period, P , and experimental data from Wiśniewska et al. (2016) (stars) and Kayshap et al. (2018) (circles) vs. height, y , (bottom) in the case of $P_d = 300$ s.

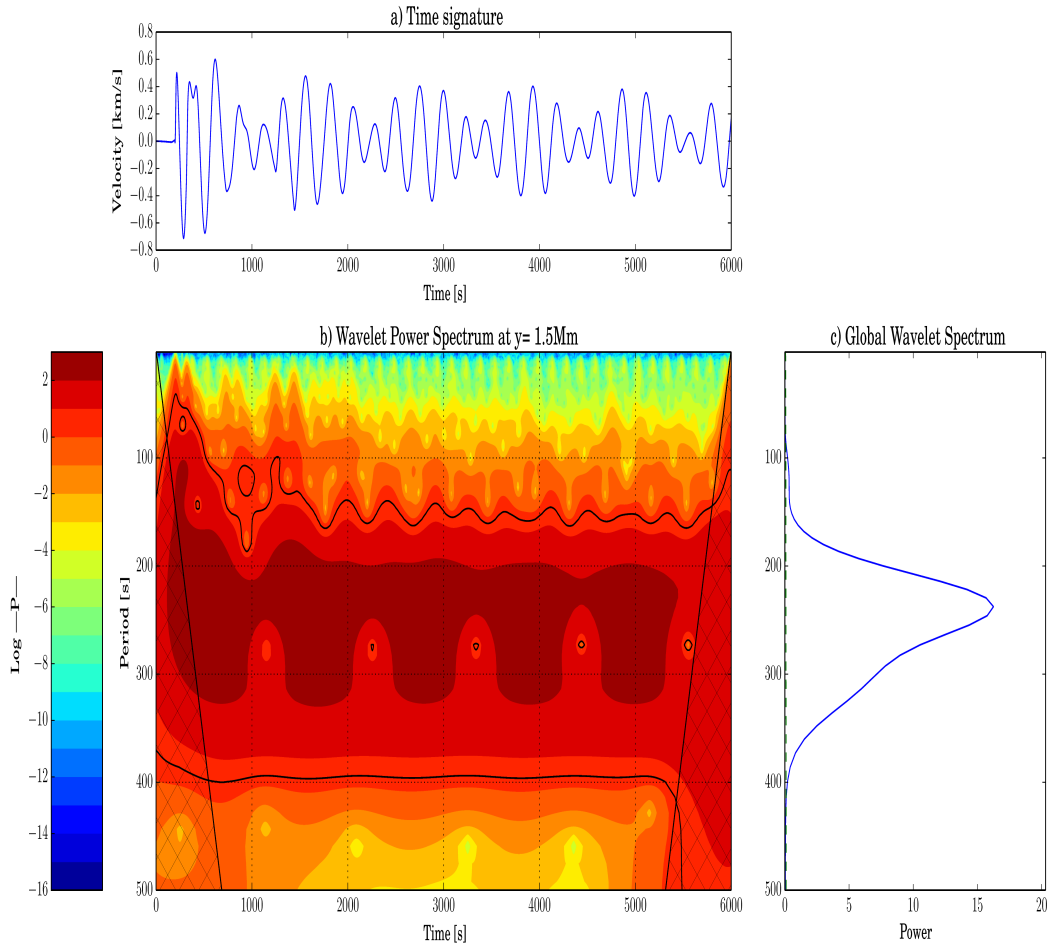


Figure 6: Time-signature for $V_{iy}(y = 1.5 \text{ Mm})$ (top), its wavelet spectrum (left-bottom), and global wavelet spectrum (right-bottom) in the case of $P_d = 300 \text{ s}$.

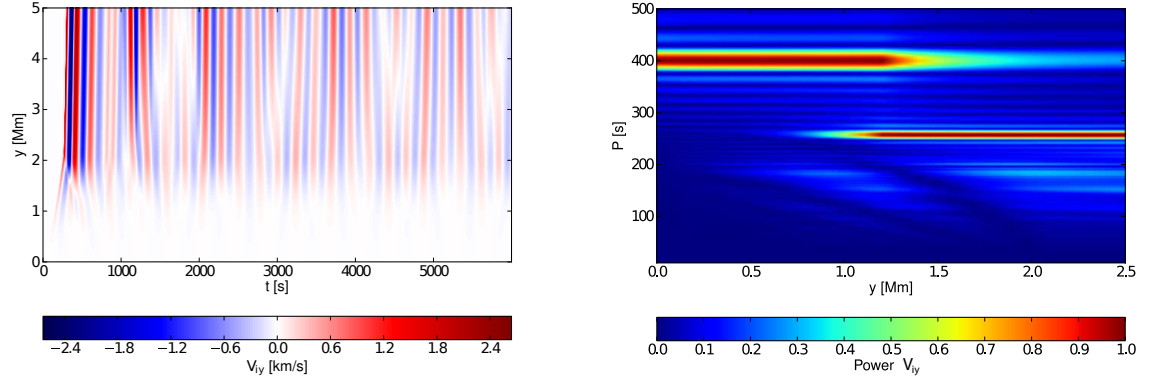


Figure 7: Time-distance plots for the ion vertical velocity, V_{iy} , and its Fourier power period, P , vs. height, y , for $P_d = 400$ s.

MAWs. Comparison of the analytical findings derived in these papers to the numerical results presented here is given and discussed. The propagation of MAWs in the solar atmosphere is affected by cutoff periods for these waves. The local cutoff period derived for the vertical magnetic field by Roberts (2006) is defined as (see Fig. 2)

$$P_m(y) = \frac{2\pi}{\Omega_m}, \quad (19)$$

where

$$\Omega_m^2(y) = c_t^2 \left\{ \frac{1}{4\Lambda^2} \left(\frac{c_t}{c_s} \right)^4 - \frac{1}{2} \gamma g \left(\frac{c_t^2}{c_s^4} \right)' + \frac{1}{c_A^2} \left(\omega_g^2 + \frac{g}{\Lambda} \frac{c_t^2}{c_s^2} \right) \right\} \quad (20)$$

and ω_g^2 denotes the squared buoyancy or Brunt-Väisälä frequency given by

$$\omega_g^2 = -g \left(\frac{g}{c_s^2} + \frac{\rho'}{\rho} \right), \quad (21)$$

with $c_t = c_s c_A / c_f$ being the 'cusp' (or tube) speed, $c_s = \sqrt{\gamma(p_{hi} + p_{hn}) / (\rho_{hi} + \rho_{hn})}$ sound speed, $c_A = B_0 / \sqrt{\mu(\rho_{hi} + \rho_{hn})}$ bulk Alfvén speed, $c_f(y) = \sqrt{c_s^2(y) + c_A^2(y)}$, $\Lambda = k_B T / (m_i + m_n)g$ and $' = d/dy$.

2.3 Periodic driver

We assume that the waves are driven by the velocity fluctuations in the lower part of the photosphere. Since typical periods of these fluctuations are about 5

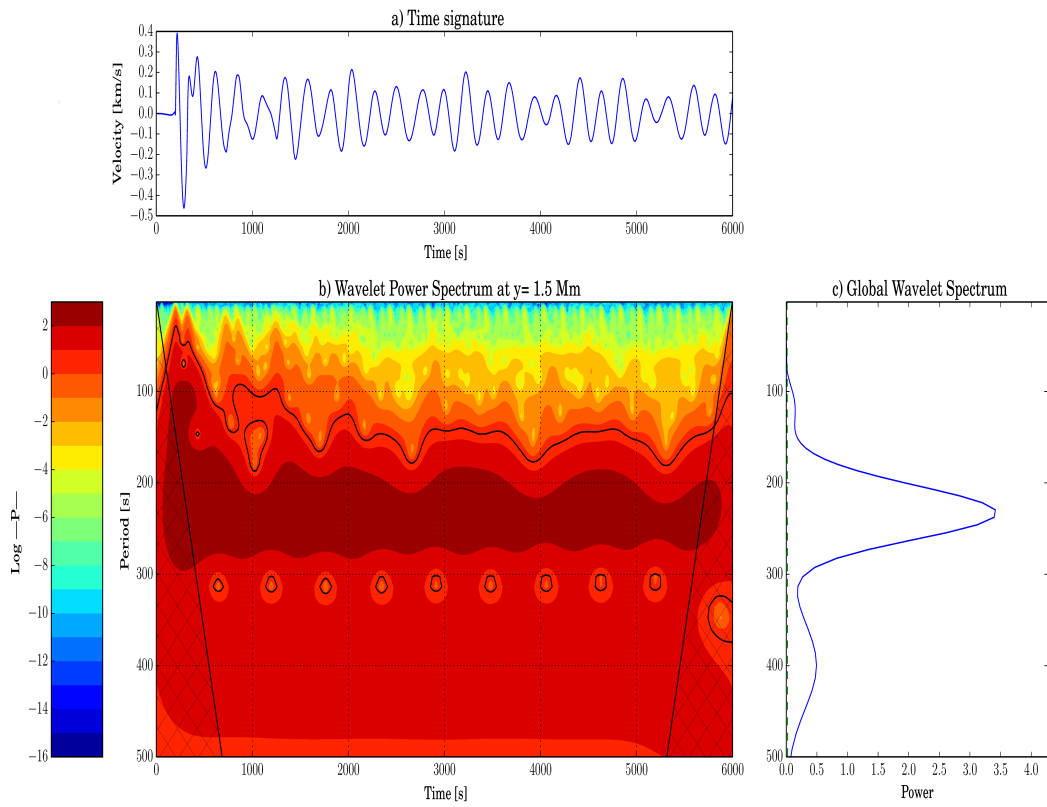


Figure 8: Time-signature for $V_{iy}(y = 1.5 \text{ Mm})$ (top), its wavelet spectrum (left-bottom), and global wavelet spectrum (right-bottom) in the case of $P_d = 400 \text{ s}$.

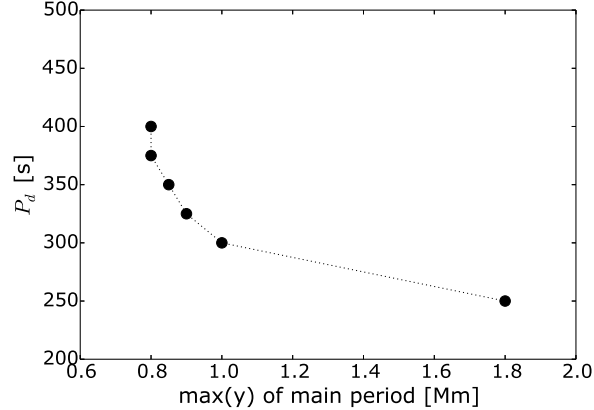


Figure 9: Main Fourier period, P_m , for V_{iy} vs. maximum value of y at which this period is present in the case of $B_y = 11.4$ G.

min, we set a monochromatic driver at the height of $y = 0$ Mm operating with the period close to $P = 300$ s. We develop a numerical model for the wave propagation and this model generalizes the previous MHD studies of monochromatic MAWs waves performed by Kraškievicz et al. (2019).

We perturb the solar atmosphere by the driver in the y -components of ion and neutral velocities given by

$$V_{iy}(y = 0, t) = V_{ny}(y = 0, t) = V_0 \sin\left(\frac{2\pi t}{P_d}\right), \quad (22)$$

where $V_0 = 0.025 \text{ km s}^{-1}$ is the amplitude of the driver and P_d stands for its period. Here we consider wave-periods equal or longer than 200 s. For such values of P_d collisions between ions and neutrals are not expected to play any significant role in wave damping and consequently in thermalization of their energy. However, frequent ion-neutral collisions in the lower atmospheric layers result in strong ion-neutral coupling in the photosphere and less frequent collisions in weak coupling in the top chromosphere and the low corona, which affects cutoff wave-periods.

The driver generates neutral acoustic and ion MAWs waves propagating through the photosphere and then through the chromosphere towards the corona. We study these waves by tracing the y -components of ion and neutral velocities and their mass densities. We aim is to show that some waves of their wave-periods larger than 300 s are evanescent and they are not able to reach the solar corona. Note that internal gravity waves are removed from the model by considering the background medium such as 1D plasma, which means that $\partial/\partial x = \partial/\partial z = 0$.

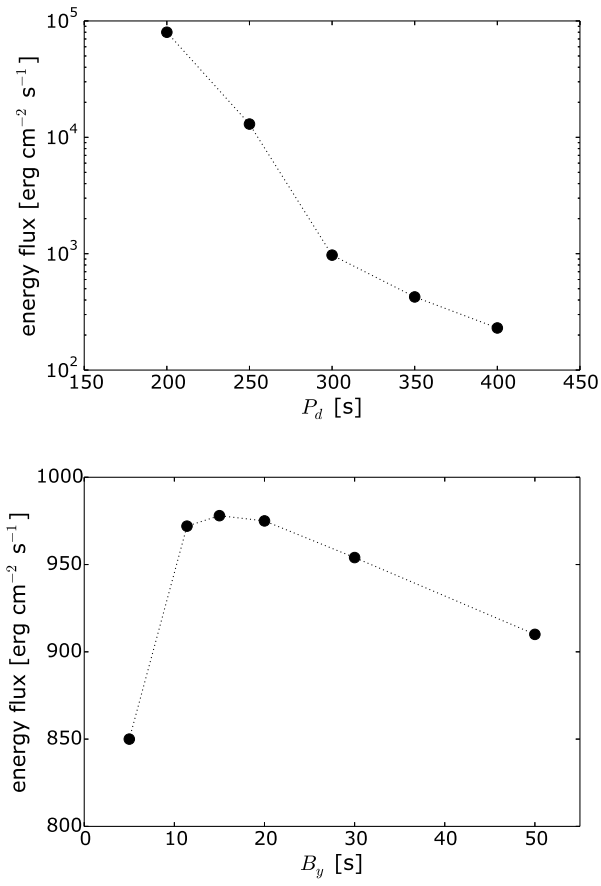


Figure 10: Energy flux vs. the driving period for $B_y = 11.4$ G (top) and vs. magnetic field for $P_d = 300$ s (bottom), evaluated at $y = 1.9$ Mm.

3 NUMERICAL RESULTS

We perform numerical simulations of the MAWs in a partially ionized and weakly magnetized solar atmosphere by using the JOANNA code (Wójcik et al. 2018). The code is based on the original work by Leake et al. (2012), who considered a two-fluid model of ions and neutrals as separate fluids. This code was extensively tested in Wójcik et al. (2019, 2020) and in Murawski, Musielak & Wójcik (2020); the latter paper reports on a good agreement between the results obtained by the code and the observations.

We present results of numerical simulations with use of a 1D uniform grid of its finest size of $\Delta y = 5$ km between $y = 0$ and $y = 5.12$ Mm. Higher up the grid stretches up with height until the top boundary which is located at $y = 60$ Mm. At the bottom and top boundaries, we set and hold fixed in time all plasma quantities to their equilibrium values. The only exception is the bottom boundary at which we overlay the equilibrium quantities by the driver, specified by Eq. (22). This means that the presented results are valid for the photosphere and chromosphere, and that they can be used to establish ranges of waves that may carry energy up to the corona.

We focus on waves with periods of a few hundred seconds because for these waves the ion-neutral collisions are ineffective in thermalization of the wave energy. On the other hand, if wave periods are an order of magnitude shorter, then their periods become close to the ion-neutral collision time (e.g., Popescu Braileanu et al. 2019), and therefore these waves are not considered here. Since waves of short periods are mainly responsible for the heating of the solar chromosphere, the latter is not discussed in this paper, but instead the presented results are focused on the wave energy transport to the solar corona. In the following, we describe in detail the obtained numerical results and discuss their implications for solar physics.

3.1 The case of $P_d = 200$ s

In Fig. 3 (top), we show the time-distance plot for the ion vertical velocity, V_{iy} , for the wave-period, $P_d = 200$ s. It is seen that the signal evolution remains essentially unchanged in time for a fixed height, and that the wave signals propagate through the photosphere and chromosphere to the corona. Figure 3 (bottom) demonstrates the Fourier period, P vs. height, y in which we clearly see the main period $P_d = 200$ s and also $P_{\text{cutoff}} = 230$ s, albeit with less power, for $1.0 \text{ Mm} < y < 1.5 \text{ Mm}$. The same period we can infer from the formula $P_{\text{cutoff}} = P_{\text{mod}} P_d / (P_{\text{mod}} - P_d)$, where the modulation period, $P_{\text{mod}} \approx 1470$ s, is estimated from Fig. 4 ((a) panel). The period of 230 s is consistent with the cutoff wave-period for MAWs at $y = 1.5$ Mm (Fig. 2), and it is exited together with the driver period.

In Fig. 4, we demonstrate the time-signature of $V_{iy}(y = 1.5 \text{ Mm})$ (top) and the corresponding wavelet spectra (bottom) for the wave-period $P_d = 200$ s. The time-signature exhibits the modulations with P_{mod} (top), which is discernible in the wavelet spectrum for $70 \text{ s} \lesssim t \lesssim 590 \text{ s}$ (bottom-left). The presented results

reinforce those shown in Fig. 3. The main implication of these results is that the propagating wave pattern is seen for the waves of this period in the solar photosphere and chromosphere, which means that these waves carry most of their energy directly to the solar corona.

Let us point out that as in the case of $P_d = 200$ s the differences between the neutral and ion velocity periodograms are very small, we show here only the ion case.

3.2 The case of $P_d = 300$ s

Figure 5 presents time-distance plot for V_{iy} (top) and its Fourier spectrum (bottom) for $P_d = 300$ s. The presented results show that the waves with periods of $P = 300$ s cannot reach the solar corona as their power spectrum significantly decreases with height in the middle chromosphere. Moreover, it is also seen that shorter period waves appear. These waves correspond to the local cutoff with the strongest signal associated with $P_{\text{cutoff}} \approx 240$ s, observed at $y > 1$ Mm in Figs. 2 and 5. A comparison of these wave periods with the observational data of Wiśniewska et al. (2016) and Kayshap et al. (2018) reveals an agreement at some points. Hence, the qualitative similarity between the numerical results and the observational findings confirms that ion-neutral collisions are an efficient mechanism of energy release.

Figure 6 illustrates time-signature for $V_{iy}(y = 1.5 \text{ Mm})$ (top) and the corresponding wavelet spectra (bottom). Despite different wave periods displayed in Figs. 4 and 6, the wave evolution remains apparently unchanged. However, the wave profile is altered in comparison to the driving signal, with clear signs of modulation seen in the time-signature (top). The modulation period, P_{mod} , in this case can be estimated from Fig. 6 (top) as $P_{\text{mod}} \approx 1200$ s, giving $P_{\text{cutoff}} = P_{\text{mod}}P_d/(P_{\text{mod}} + P_d) \simeq 240$ s. This value is close to 230 s which was estimated for $P_d = 200$ s and it is present for $y > 1$ Mm in Fig. 2.

3.3 The case of $P_d = 400$ s

Figure 7 presents time-distance plot for V_{iy} (top) and its Fourier power spectrum (bottom) for $P = 400$ s. Comparison to the results of previous figures demonstrates that these waves can reach only the atmospheric height $y \simeq 1.3$ Mm. As a result, these waves cannot become propagating until they reach the solar corona, and the waves with period of $P_{\text{cutoff}} \approx 255$ s are excited at about $y = 1.2$ Mm (bottom). This period is close to cutoff periods seen in Fig. 2 for $y > 1$ Mm.

Note that the results presented in Fig. 7 (bottom) reveal at the top chromosphere the wave-periods which are much lower than the driving period of $P_d = 400$ s. These wave-periods are in the range of 200 – 300 s and they support the results given by Fleck & Schmitz (1991) and Kalkofen et al. (1994). According to these authors, any P_d higher than the local atmospheric cutoff period initially oscillates with its local cutoff and later on the oscillations evolve to reach P_d (see Fig. 8, left-bottom). The global wavelet spectrum reveals that

the signal at $P = P_d = 400$ s is much lower than the signal at $P \approx 230$ s (right-bottom), which agrees with Fig. 7 (bottom) which shows that for $y > 1.5$ Mm the signal corresponding to $P \simeq 230$ s is stronger than that for $P = 400$ s.

As expected from our previous results obtained for the waves with periods of 200 s and 300 s, the waves with their periods of 400 s cannot reach the solar chromosphere because their power spectrum is significantly reduced in the solar chromosphere and its shape is altered, so the waves become evanescent. By using the latter wave property, we were able to determine the cutoff period for the waves in the solar chromosphere and corona, and use it to establish the conditions for the wave propagating in these layers of the solar atmosphere.

3.4 Parametric studies

Figure 9 displays main Fourier period for V_{iy} vs. maximum value of y at which this period is present, i.e. $P_m = P_d$ for $y < \max(y)$; for $y > \max(y)$ the dominant period in the Fourier spectrum is lower than the driving period P_d . Note the fast fall-off of P_m in the range of $0.75 \text{ Mm} < y < 1 \text{ Mm}$ which means that the driver with its wave-period P_d higher than about 300 s excites evanescent magnetoacoustic waves reaching the low chromosphere. Such a drastic decline of wave wave-periods was already detected in the numerical data for stochastically excited magnetoacoustic-gravity waves in a quiet region of the solar atmosphere, see Fig. 4 in Krařkiewicz and Murawski (2019), and in the observational data of Wiřniewska et al. (2016).

We discuss now the energy flux which is approximated by the following formula:

$$F_E \approx \frac{1}{2} \rho_i \mathbf{V}_i^2 c_s. \quad (23)$$

We evaluate this flux at $y = 1.9$ Mm. Figure 10 illustrates F_E vs. the driving period, P_d , (top) and magnetic field, B_y , (bottom). Note that F_E declines with P_d , meaning that shorter wave-period waves carry more energy than longer wave-period waves (top). The variation of F_E with B_y reveals that for $B_y = 5$ G $F_E \approx 850 \text{ erg cm}^{-2} \text{ s}^{-1}$. For higher values of B_y F_E grows, attaining its local maximum at $B_y = 15$ G, and then F_E declines to $F_E \approx 910$ G for $B_y = 50$ G (bottom). These energy fluxes can be compared with the data in Tab. 1 from Withbroe & Noyes (1977) according to which total energy loss is $3 \cdot 10^5 \text{ erg cm}^{-2} \text{ s}^{-1}$. The data of Fig. 10 shows that F_E is close to $1 \cdot 10^5 \text{ erg cm}^{-2} \text{ s}^{-1}$ for $P_d = 200$ s and $B_y = 11.4$ G (top). As for other considered values F_E is lower than the required values to balance energy losses in the top chromosphere (Withbroe & Noyes 1977), we conclude that only the monochromatic driver with its period $P_d = 200$ s and $B_y = 11.4$ G is able to provide the required energy flux to heat the top chromosphere.

3.5 Oscillations in mass densities

It is noteworthy that in the limit of long wave-period waves, that is discussed in this paper, ions and neutrals acquire similar velocities, $\mathbf{V}_i \simeq \mathbf{V}_n$. As a result

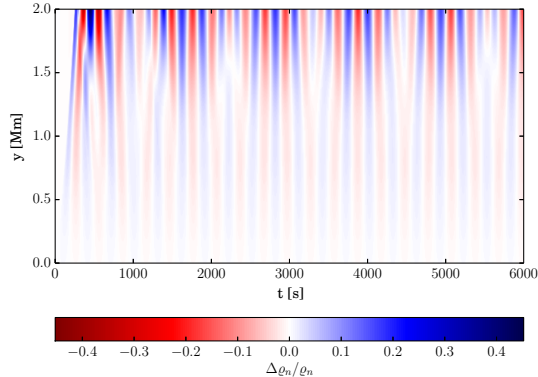


Figure 11: Time-distance plots for $\Delta\rho_n/\rho_n$ and $P_d = 300$ s.

of that the ion-neutral drag force is negligible and the collisional heating is marginal. Besides, wave dispersion is minimal (e.g., Zaqarashvili et al. 2011) and the two-fluid equations approach is limited to the two-species equations (e.g. Terada et al. 2009). These two-species equations reveal potentially different evolution of ion and neutral mass densities. Therefore, we discuss this evolution here.

Figure 11 describes the time-distance plot for relative perturbations of the neutral mass density, $\Delta\rho_n/\rho_n = (\rho_n - \rho_{n0})/\rho_n$, from the equilibrium state. The pattern is similar to $V_{iy}(t, y)$ but the investigation of the Fourier power spectrum shows some different behaviour of ions from neutrals (Fig. 12). More significant difference is seen in Fig. 13 which shows time-signatures for ρ_i and ρ_n , collected at $y = 1.5$ Mm (a panels), the corresponding wavelet spectra (left-bottom panels), and the global wavelet spectra (right-bottom panels). These global wavelet spectra reveal the excited signal of $P = 150$ s for ions (top) and lack of that for neutrals (bottom panel) at $y = 1.5$ Mm. These different oscillations of ρ_i and ρ_n from those in V_{iy} are not surprising as even in the case of linear MHD mass density is governed by a different evolution equation than vertical velocity is (Roberts 2006).

The presented results show that the waves with periods of 300 s cannot reach the solar corona because of their spectrum decreases significantly in the middle chromosphere. This clearly shows the effects of the solar chromosphere on the waves of this period, which is very different than the effects of the chromosphere on the waves with periods of 200 s. Our results also demonstrate the changes between the driven and propagating wave profiles in the solar chromosphere. We also report on differences in the behaviour of ions and neutrals, which are revealed in their different oscillations, but we point out that these differences have already been observed before.

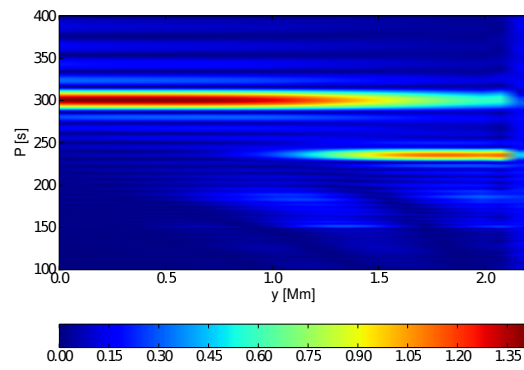
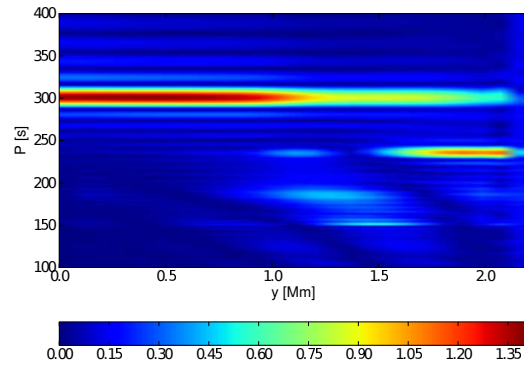


Figure 12: Fourier period, P , vs. height, y , for ϱ_i (top) and ϱ_n (bottom) in the case of $P_d = 300$ s.

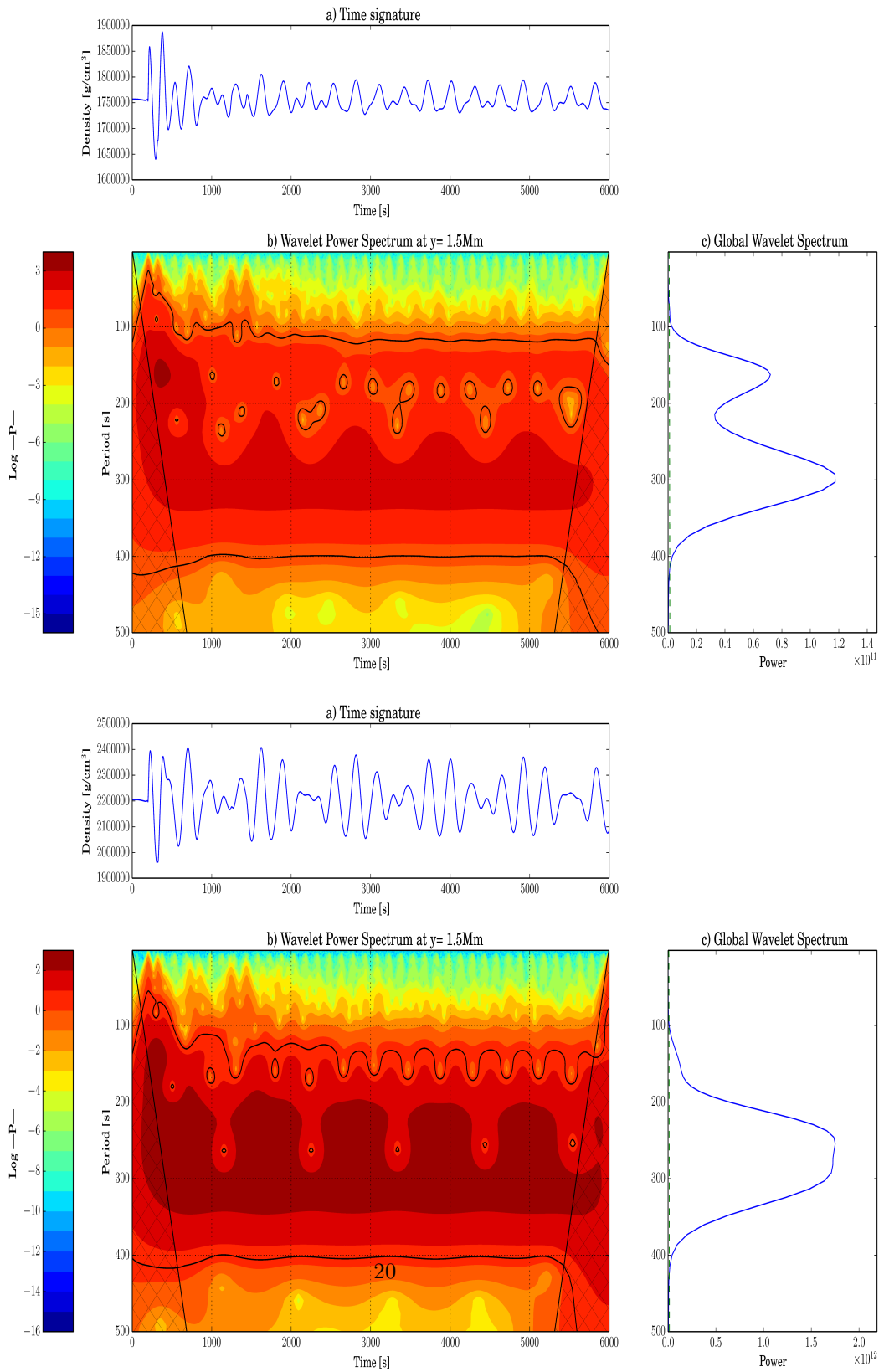


Figure 13: Wavelet spectrum for q_i (top) and q_n (bottom), collected at $y = 1.5 \text{ Mm}$, in the case of $P_d = 300 \text{ s}$.

4 CONCLUSIONS AND SUMMARY

We performed 1D numerical simulations of propagation of neutral acoustic and ion magnetoacoustic two-fluid waves in the partially ionized lower solar atmosphere, consisting of ion+electron and neutral fluids, which are coupled by ion-neutral collisions. The considered atmosphere was assumed to be permeated by a uniform vertical magnetic field and the waves were excited by a monochromatic driver located at the bottom of the solar photosphere. We investigated variations of wave-periods with height in the solar atmosphere, which allowed us to find the wave cutoffs and determine the conditions for the wave propagation.

Our main results demonstrate that waves with different wave-periods than those long wave-periods generated by the driver are present and that their vertical propagation is strongly affected by the solar atmosphere, which filters out the 300 s (and longer) waves and makes some of these waves evanescent. By identification of the evanescent waves we were able to find the wave cutoffs and their variations in the solar atmosphere, and use them to determine the propagation conditions for the considered waves. Then, we used the propagation conditions to find periods of waves that may carry their energy from the solar surface to the corona. Additionally, we showed that according to the analytical predictions (e.g. Roberts 2006) oscillations in mass densities exhibit different wave period spectra than in their vertical velocity component.

Finally we mention that a two-fluid model describes dynamics of two fluids, such as ions+electrons and neutrals. An MHD model does not distinguish between these two fluids and therefore it is inferior to a two-fluid model. Our results reveal that Fourier spectra of excited oscillations of these two fluids differ one from another and they depend on whether these spectra are drawn for vertical velocities (see Sect. 3) or for mass densities (see Appendix). Obviously for wave-periods much larger than ion-neutral collision time the spectra for vertical velocities are similar in the framework of MHD and the two-fluid model.

ACKNOWLEDGMENTS

The JOANNA code was developed by Darek Wójcik with some contribution from Luis Kadowaki and Piotr Wołoszkiewicz. KM's work was done within the framework of the projects from the Polish Science Center (NCN) Grant No. 2020/37/B/ST9/00184.

DATA AVAILABILITY

The data underlying this article are available in the article and in its online supplementary material.

REFERENCES

- Avrett, E. H. & Loeser, R. 2008, *ApJS*, 175, 229
- Ballester, J. L., Alexeev, I., Collados, M., et al. 2018, *Space Science Reviews*, 214, 58B
- Cally, P. S., & Hansen, S. C. 2011, *ApJ*, 738, 119
- Chmielewski, P., Srivastava, A. K., Murawski, K., et al. 2013, *MNRAS*, 428, 40

Defouw, R. J. 1976, *ApJ*, 209, 266
 Felipe, T., Kuckein, C., & Thaler, I. 2018, *A&A*, 617, A39
 Fleck, B., & Schmitz, F. 1991, *A&A*, 250, 235
 Fleck, B., & Schmitz, F. 1993, *A&A*, 273, 671
 Gough D. O. 1977, *ApJ*, 214, 196
 Kalkofen W., Rossi P., Bodo G., Massaglia S. 1994, *A&A*, 284, 976
 Kayshap, P., Murawski, K., Srivastava, A. K., et al. 2018, *MNRAS*, 479, 5512
 Kraśkiewicz, J.K. & Murawski, K. 2019, *MNRAS*, 482, 3244
 Kraśkiewicz, J.K., Murawski, K., & Musielak, Z.E. 2019, *A&A*, 623, A62
 Kuźma, B., Wójcik, D., Murawski, K. 2019, *A&A*, 878, 81
 Kuźma, B., Murawski, K., & Musielak, Z.E. 2022, submitted to *MNRAS*
 Lamb, H. 1909, *Proc. Lond. Math. Soc.*, 7, 122
 Lamb, H. 1910, *Proc. R. Soc. London*, A, 34, 551
 Lamb, H. 1945, *Hydrodynamics*, Dover Publications, New York
 Leake, J. E., Lukin, V. S., Linton, M. G., Meier, E. T. 2012, *ApJ*, 760, 109
 Martínez-Sykora, J., Pontieu, B. D., Hansteen, V. H., et al. 2017, *Science*, 356, 1269
 Murawski, K., Musielak, Z. E., Konkol, P., et al. 2016, *ApJ*, 827, 37
 Musielak, Z. E., Musielak, D. E., & Mobashi, H. 2006, *Phys. Rev. E*, 73, 036612-1
 Maneva, Y.G., Alvarez Laguna, A., Lani, A., & Poedts, S. 2017, *ApJ*, 836, 197
 Murawski, K., & Zaqarashvili, T. V. 2010, *A&A*, 519, 8
 Murawski, K., & Musielak, Z. E. 2010, *A&A*, 518, A37
 Murawski, K., & Musielak, Z.E. 2016, *MNRAS*, 463, 4433
 Murawski, K., Musielak, Z.E., Wójcik, D. 2020, *ApJL*, 896 L1
 Musielak, Z. E. 1990, *ApJ*, 351, 287
 Musielak Z. E., Moore R., 1995, *ApJ*, 452, 434
 Musielak, Z. E., Routh, S., & Hammer, R. 2007, *ApJ*, 659, 650
 Musielak Z. E., Musielak, D. E., Mobashi H. 2006, *Phys. Rev. E*, 73, 036612-1
 Narain, U., & Ulmschneider, P. 1996, *Space Sci. Rev.*, 75, 453
 Oliver, R., Soler, R., Terradas, J., & Zaqarashvili, T. V. 2016, *ApJ*, 818, 128
 Perera, H. K., Musielak, Z. E., & Murawski, K. 2015, *MNRAS*, 450, 3169
 Priest, E. R. 2014, *Magnetohydrodynamics of the Sun*, Cambridge University Press, Cambridge
 Popescu Braileanu, B., Lukin, V. S., Khomenko, E., et al. 2019, *A&A*, 627, A25
 Rae, I. C., & Roberts, B. 1982, *ApJ*, 256, 761
 Roberts, B. 1991, *Geophysical and Astrophysical Fluid Dynamics*, 62, 83
 Roberts, B., & Ulmschneider, P. 1997, *European Meeting on Solar Physics*, 75
 Roberts, B. 2004, *Proceedings of 'SOHO 13 Waves, Oscillations and Small-scale Transients Events in the Solar Atmosphere: Joint View from SOHO and TRACE'*, Compiled by: H. Lacoste, p. 1
 Roberts, B. 2006, *Phil. Trans. R. Soc. A*, 364, 447
 Rogers, F. J. & Nayfonov, A. 2002, *ApJ*, 576, 1064
 Routh S., Musielak Z. E. 2014, *Astronomische Nachrichten*, 335, 1043
 Routh, S., Musielak, Z. E., & Hammer, R. 2010, *ApJ*, 709, 1297
 Routh, S., Musielak, Z.E., Sundar, M.N., Joshi, S.S., & Charan, S. 2020, *As-*

trohys. & Space Sci., 365, 139
Schmitz, F., & Fleck, B. 1992, A&A, 260, 447
Stark, B.A., & Musielak, Z.E. 1993, ApJ, 409, 450
Terada, N., Shinagawa, H., Tanaka, T., Murawski, K., Terada, K. 2009, JGR,
114, A09208
Vögler, A. 2004, Three-dimensional simulations of magnetoconvection in the
solar photosphere (Copernicus)
Vranjes, J., & Krstic, P. 2013, App, 554, A22
Wiśniewska, A., Musielak, Z. E., Staiger, J., Roth M. 2016, ApJ, 819, L23
Withbroe, G. L. & Noyes, R. W. 1977, Annual Rev. Astr. Astrophys., 15.
(A78-16576 04-90) Palo Alto, Calif., Annual Reviews, Inc., 1977, p. 363
Wójcik, D., Murawski, K., & Musielak, Z. E. 2018, MNRAS, 481, 262
Wójcik, D., Murawski, K., & Musielak, Z.E. 2019, ApJ, 882, 32W
Wójcik, D., Kuźma, B., Murawski, K., Musielak, Z.E. 2020, A&A, 635, A28
Zaqarashvili, T.V., Khodachenko, M.L., Rucker, H.O. 2011, A&A, 529, A82